

632 **Appendix A. Supplementary Material**

633 *Appendix A.1. Histological sectioning*

634 After diffusion tensor imaging, the injected specimens underwent serial histological section-
635 ing. The tissue samples were fixed in 10% neutral buffered formalin, immersed in 70%
636 ethanol, and embedded in paraffin. 20 5- μ m sections were obtained with a step size of 300
637 μ m, spanning across the thickness of each specimen, and Masson's trichrome staining was
638 used to identify the myofibers, collagen fibers, and hydrogel. Sections were photographed
639 with a Nikon SMZ 800 microscope. Histology was performed at Histoserv, Inc. (German-
640 town, MD).

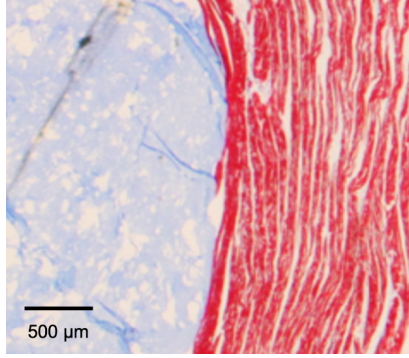


Fig. A.1: Histology. Masson trichrome stain of injected myocardium showing interface of tissue (red) and hydrogel (blue).

641 *Appendix A.2. Maximum tangent modulus vs. injection volume*

642 Maximum tangent modulus m was determined using the reaction forces computed on the
 643 mesh boundaries in all deformation modes for each of the parametric simulations. Simula-
 644 tions varied by injection placement in the transmural direction, injection volume, hydrogel
 645 stiffness, and post-MI myocardium material parameters. We simulated the myocardium
 646 without hydrogel inclusion to emulate the control response, using $n = 3$ meshes with identi-
 647 cal fiber orientation mappings and material properties. To assess maximum tangent modulus
 648 m as a function of injection volume, group averages of all transmural placements (endo, mid,
 649 epi) were computed at each volume (0%, 1.5%, 5%, and 17%), $n = 3$ for each group. These
 650 computations were done separately for both post-MI time points (0 WK and 4 WK).

651 Group-averaged m was displayed as mean \pm standard error of the mean (SEM). We
 652 used a two sample t-test to compare group averages, and p-values ≤ 0.05 were considered
 653 statistically significant. All statistical analysis was performed using MATLAB.

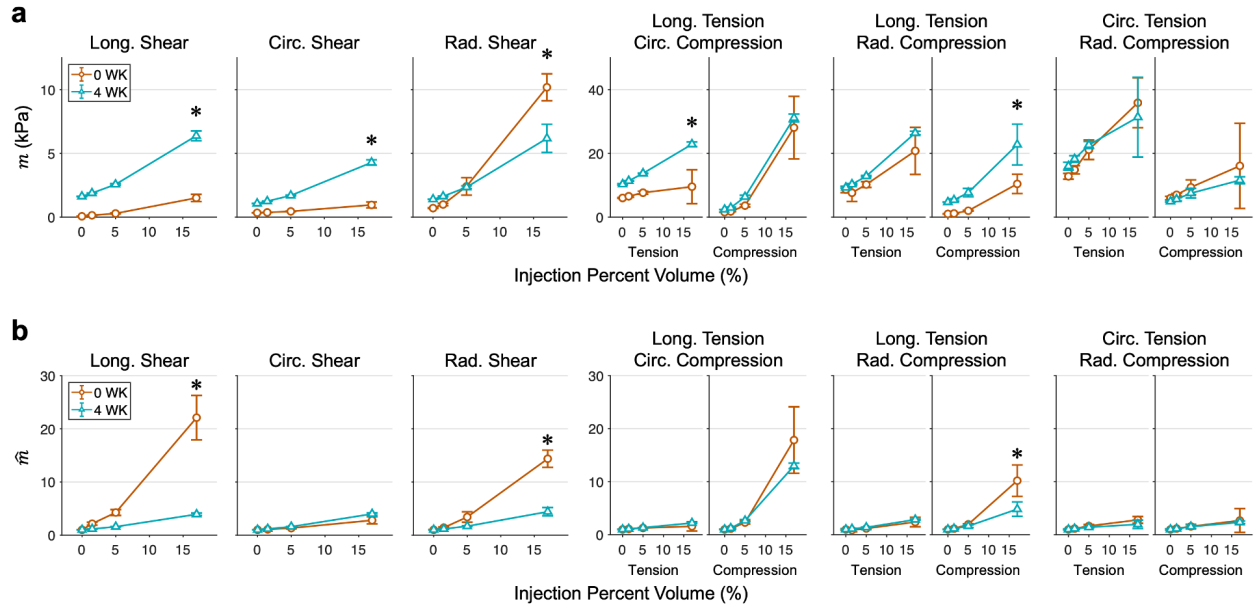


Fig. A.2: Maximum tangent modulus as a function of injection volume. (a) Absolute m and (b) normalized \hat{m} derived from finite element simulations of injected myocardium with hydrogels of increasing volume for the 0 WK (orange) and 4 WK (blue) post-MI time points. Quantities displayed as Mean \pm SEM. Significant differences between the 17% injection of the 0 WK and 4 WK time points indicated with $*p \leq 0.05$.

654 *Appendix A.3. Maximum principal strain vs. injection volume*

655 At maximum deformation, the Green-Lagrange strain tensor \mathbf{E} was calculated for all my-
 656 ocardium elements within a spherical region of interest centered in the cube domain, ex-
 657 cluding both distal myocardium elements and hydrogel elements. A volume-averaged strain
 658 tensor $\bar{\mathbf{E}}$ was obtained by averaging each corresponding component of \mathbf{E} across all elements
 659 in the region of interest and used to determine the maximum principal strain for the my-
 660 ocardium in each deformation mode. The maximum principal strain in each deformation
 661 mode E_1 was evaluated for all placement-volume combinations at both post-MI time points.

662 To assess maximum principal strain E_1 as a function of injection volume, group averages
 663 of all transmural placements (endo, mid, epi) were computed at each volume (0%, 1.5%, 5%,
 664 and 17%), $n = 3$ for each group. These computations were done separately for both post-MI
 665 time points (0 WK and 4 WK). Group-averaged E_1 was displayed as mean \pm standard error
 666 of the mean (SEM).

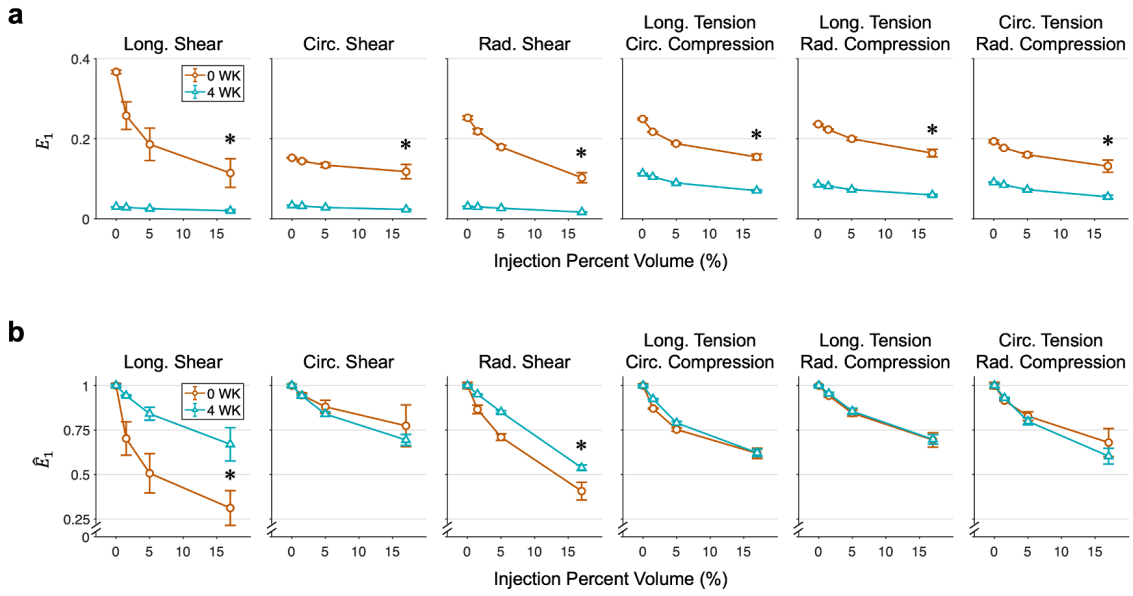


Fig. A.3: Maximum principal strain as a function of injection volume. (a) Absolute E_1 and (b) normalized \hat{E}_1 derived from finite element simulations of injected myocardium with hydrogels of varying placement and volume for the 0 WK (orange) and 4 WK (blue) post-MI time points. Quantities displayed as Mean \pm SEM. Significant differences between the 17% injection of the 0 WK and 4 WK time points indicated with $*p \leq 0.05$.

667 *Appendix A.4. Maximum principal strain vs. injection stiffness*

668 The maximum principal strain in each deformation mode E_1 was evaluated as a function of
 669 hydrogel modulus for the mid-placed inclusion of 17% cuboid volume. Evaluating changes
 670 in maximum principal strain as a function of hydrogel stiffness was performed using only the
 671 17% injection volume with a mid placement.

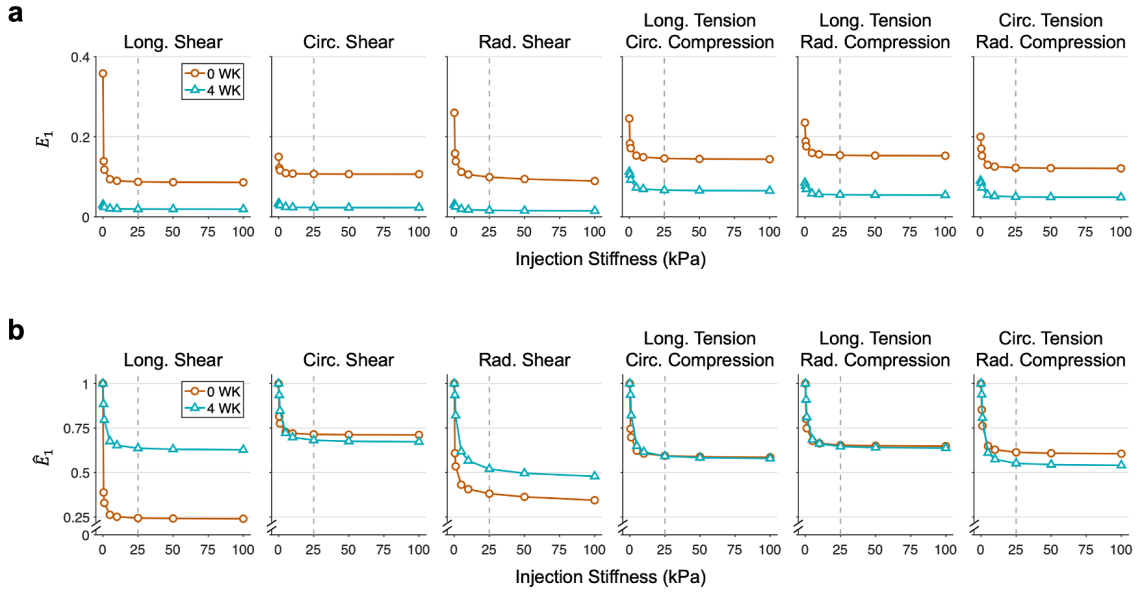


Fig. A.4: Maximum principal strain as a function of injection stiffness. (a) Absolute E_1 and (b) normalized \hat{E}_1 derived from finite element simulations of the 0 WK and 4 WK post-MI time points undergoing optimal deformations modes with increasing hydrogel modulus. The largest injection volume (17%) at mid placement is evaluated. Further increases in modulus have a minimal effect beyond stiffness values indicated by the dotted gray lines.